

Particle Acceleration on Megaparsec Scales in a Merging Galaxy Cluster*

Reinout J. van Weeren,^{1*} Huub J. A. Röttgering,¹ Marcus Brüggen², Matthias Hoeft³

¹Leiden Observatory, Leiden University,

P.O. Box 9513, NL-2300 RA, Leiden, The Netherlands

²Jacobs University Bremen, P.O. Box 750561, 28725 Bremen, Germany

³Thüringer Landessternwarte, Sternwarte 5, 07778 Tautenburg, Germany

*To whom correspondence should be addressed; E-mail: rvweeren@strw.leidenuniv.nl

Galaxy clusters form through a sequence of mergers of smaller galaxy clusters and groups. Models of diffusive shock acceleration (DSA) suggest that in shocks that occur during cluster mergers, particles are accelerated to relativistic energies, similar to supernova remnants. Together with magnetic fields these particles emit synchrotron radiation and may form so-called radio relics. Here we report the detection of a radio relic for which we find highly aligned magnetic fields, a strong spectral index gradient, and a narrow relic width, giving a measure of the magnetic field in an unexplored site of the universe. Our observations prove that DSA also operates on scales much larger than in supernova remnants and that shocks in galaxy clusters are capable of producing extremely energetic cosmic rays.

*This is the author's version of the work. It is posted here by permission of the AAAS for personal use, not for redistribution. The definitive version was published in Science, Volume 330, 15 October 2010.

In the universe structure forms hierarchically with smaller structures merging to form bigger ones. On the largest scales, clusters of galaxies merge releasing energies of the order of 10^{64} erg on timescales of 1–2 Gyr (1, 2). During such merger events, large-scale shock waves with moderate Mach numbers of 1–5, should be created. In such shocks, DSA is expected to accelerate electrons to high energies; in the presence of a magnetic field, these particles are expected to form large regions emitting synchrotron radiation at radio wavelengths (2–4). The accelerated particles at the shock front have a power-law energy distribution which directly translates into an integrated power-law radio spectrum (flux $\propto \nu^\alpha$, with α the spectral index and ν the frequency). The slope of the particle distribution (s) in the linear test particle regime, and thus the radio spectral index ($\alpha = (1 - s)/2$), only depends on the compression ratio (r) of the shock (5, 6), with $s = (r + 2)/(r - 1)$. At the shock front, the intracluster medium (ICM) is compressed such that magnetic fields align parallel to the shock front (7). These ordered and aligned magnetic fields cause the radio emission to be highly polarized. Synchrotron and inverse Compton (IC) losses cool the radio plasma behind the shock, creating a strong spectral index gradient in the direction towards the cluster center. It has been suggested that such synchrotron emitting regions from shocks can be identified with radio relics (3, 7). These are elongated radio sources located mostly in the outskirts of massive merging galaxy clusters (8–14).

Here we present the detection of a 2 Mpc radio relic (Figs. 1, 2) located in the northern outskirts of the galaxy cluster CIZA J2242.8+5301 ($z = 0.1921$). This X-ray luminous cluster (15) ($L_X = 6.8 \times 10^{44}$ ergs $^{-1}$, between 0.1 and 2.4 keV) shows a disturbed elongated morphology in ROSAT X-ray images (16), indicative of an undergoing major merger event. The relic is located at a distance of 1.5 Mpc from the cluster center. Unlike other known radio relics, the northern relic is extremely narrow with a width of 55 kpc. Deep Westerbork Synthesis Radio Telescope (WSRT), Giant Metrewave Radio Telescope (GMRT) and Very Large Array (VLA) observations (SOM) show a clear unambiguous spectral index gradient towards the clus-

ter center (Fig. 3). The spectral index, measured over a range of frequencies between 2.3 and 0.61 GHz, steepens from -0.6 to -2.0 across the width of the narrow relic. The gradient is visible over the entire 2 Mpc length of the relic, constituting clear evidence for shock acceleration and spectral ageing of relativistic electrons in an outward moving shock. The relic’s integrated radio spectrum is a single power-law, with $\alpha = -1.08 \pm 0.05$, as predicted (5, 6). The relic is strongly polarized at the 50–60% level, indicating a well ordered magnetic field, and polarization magnetic field vectors are aligned with the relic. In the southern part of the cluster, located symmetrically with respect to the cluster center and the northern relic, there is a second fainter broader relic. The elongated radio relics are orientated perpendicular to the major axis of the cluster’s elongated X-ray emitting ICM, as expected for a binary cluster merger event in which the second southern relic traces the opposite shock wave (1). Furthermore, there is a faint halo of diffuse radio emission extending all the way towards the cluster center connecting the two radio relics (Fig. 1). This emission extends over 3.1 Mpc, making it the largest known diffuse radio source in a cluster to date.

The source cannot be a gravitational lens because it is too large and located too far from the cluster center. The morphology, spectral index, and association with a cluster exclude the possibility of the source being a supernova remnant. The source is also not related to the radio AGN located at the eastern end of the relic. High-resolution observations show this source to be detached from the relic (Fig. 2). The spectral and polarization properties are also unlike that of any known tailed radio sources (17, 18). The power-law radio spectral index, clear spectral index gradient and enormous extent, exclude the possibility the source is tracing (compressed) fossil radio plasma from a radio source whose jets are now off (19, 20). The integrated radio spectra of such fossil sources are very steep ($\alpha < -1.5$) and curved, because the radio emitting plasma is old and has undergone synchrotron and IC losses. In addition, the shell-like (and not lobe-like) morphology does not support the above scenario.

Instead, all the observed properties of the relic perfectly match that of electrons accelerated at large-scale shocks via DSA. The characteristics of the bright relic provide evidence that (at least some) relics are direct tracers of shocks waves, and a way to determine the magnetic field strength at the location of the shock using similar arguments to those that have been used for supernova remnants (21).

The configuration of the relic arises naturally for a roughly equal mass head-on binary cluster merger, without much substructure, in the plane of the sky with the shock waves seen edge-on. First, the polarization fraction of 50% or larger can only explained by an angle of less than 30 degrees between the line-of-sight and the shock surface (10). Second, because there is evidence for spectral ageing across the relic, only part of the width can be caused by projection effects.

The amount of spectral ageing by synchrotron and IC losses is determined by the magnetic field strength, B , the equivalent magnetic field strength of the cosmic microwave background (CMB), B_{CMB} , and the observed frequency. The result is a downward spectral curvature resulting in a steeper spectral index in the post-shock region (i.e., lower α). For a relic seen edge-on the downstream luminosity and spectral index profiles thus directly reflect the ageing of the relativistic electrons (22). To first approximation, the width of the relic (l_{relic}) is determined by a characteristic timescale (t_{sync}) due to spectral ageing, and the downstream velocity (v_d): $l_{\text{relic}} \approx t_{\text{sync}} \times v_d$, with $t_{\text{sync}} \propto \left(B^{1/2} / (B^2 + B_{\text{CMB}}^2) \right) \times \left(1 / (\nu(1+z))^{1/2} \right)$. Conversely, from the width of the relic and its downstream velocity, a direct measurement of the magnetic field at the location of the shock can be obtained. Using standard shock jump conditions, it is possible to determine the downstream velocity, from the Mach number and the downstream plasma temperature.

The spectral index at the front of the relic is -0.6 ± 0.05 which gives a Mach number of $4.6_{-0.9}^{+1.3}$ for the shock (14) in the linear regime. Using the $L_X - T$ scaling relation for clusters (23)

we estimate the average temperature of the ICM to be ~ 9 keV. Behind the shock front the temperature is likely to be higher. Temperatures in the range between 1.5 and 2.5 times the average value have previously been observed (24). The derived Mach number and the advocated temperature range, imply downstream velocities between 900 and 1,200 km s⁻¹ (we used an adiabatic exponent of 5/3). For the remainder we will adopt a value of 1,000 km s⁻¹. Using the redshift, downstream velocity, spectral index, and characteristic synchrotron timescale we have for the width of the relic

$$l_{\text{relic}, 610 \text{ MHz}} \approx 1.2 \times 10^3 \frac{B^{1/2}}{B^2 + B_{\text{CMB}}^2} \text{ [kpc]}, \quad (1)$$

with B and B_{CMB} in units of μGauss . Because B_{CMB} is known, the measurement of l_{relic} from the radio maps, directly constrains the magnetic field. From the 610 MHz image (the image with the best signal to noise ratio and highest angular resolution), the relic has a deconvolved width (full width at half maximum) of 55 kpc (Fig. 4). Because Eq. 1 has two solutions, the strength of the magnetic field is 5 or 1.2 μGauss . However, projection effects can increase the observed width of the relic and affect the derived magnetic field strength. Therefore, the true intrinsic width of the relic could be smaller, which implies that $B \geq 5$ or $\leq 1.2 \mu\text{Gauss}$ (Eq. 1). We investigated the effects of projection using a curvature radius of 1.5 Mpc, the projected distance from the cluster center. Instead of using Eq. 1, we computed full radio profiles (25) for different angles subtended by a spherical shock front into the plane of the sky (Ψ ; the total angle subtended is 2Ψ for a shell-like relic). The profile for $\Psi = 10$ deg and $B = 5 \mu\text{Gauss}$ agrees best with the observations (Fig. 4). For $\Psi = 15$ deg, B is 7 or 0.6 μGauss . Values of Ψ larger than ~ 15 deg are ruled out. Lower limits placed on the IC emission (26, 27) and measurements of Faraday rotation (28) indicate magnetic fields higher than $\sim 2 \mu\text{Gauss}$. We therefore exclude the lower solutions for the magnetic field strength and conclude that the magnetic field at the location of the bright radio relic is between 5 and 7 μGauss .

Magnetic fields within the ICM are notoriously difficult to measure. No methods have yielded precise magnetic field strengths as far from the center as the virial radius; only lower limits using limits on IC emission have been placed. Equipartition arguments have been used (9, 10, 12, 14) but this gives only a rough estimate for the magnetic field strength and it relies on various assumptions that cannot be verified. The value of $5\text{--}7 \mu\text{Gauss}$ we find shows that a substantial magnetic field exists even far out from the cluster center.

Because radio relics directly pinpoint the location of shock fronts they can be used to get a complete inventory of shocks and their associated properties in galaxy clusters, important to understand the impact of shocks and mergers on the general evolution of clusters. Because less energetic mergers are more common and have lower Mach numbers, there should be many fainter relics with steep spectra which have currently escaped detection. Interestingly, these large-scale shocks in galaxy clusters have been suggested as acceleration sites for highly relativistic cosmic rays (29). As the radiation losses for relativistic cosmic ray protons are negligible, the maximum energy to which they can be accelerated is only limited by the lifetime of the shock, which can last for at least 10^9 yr. This means that in merging clusters protons can be accelerated up to extreme energies of 10^{19} eV, much higher than that in supernova remnants.

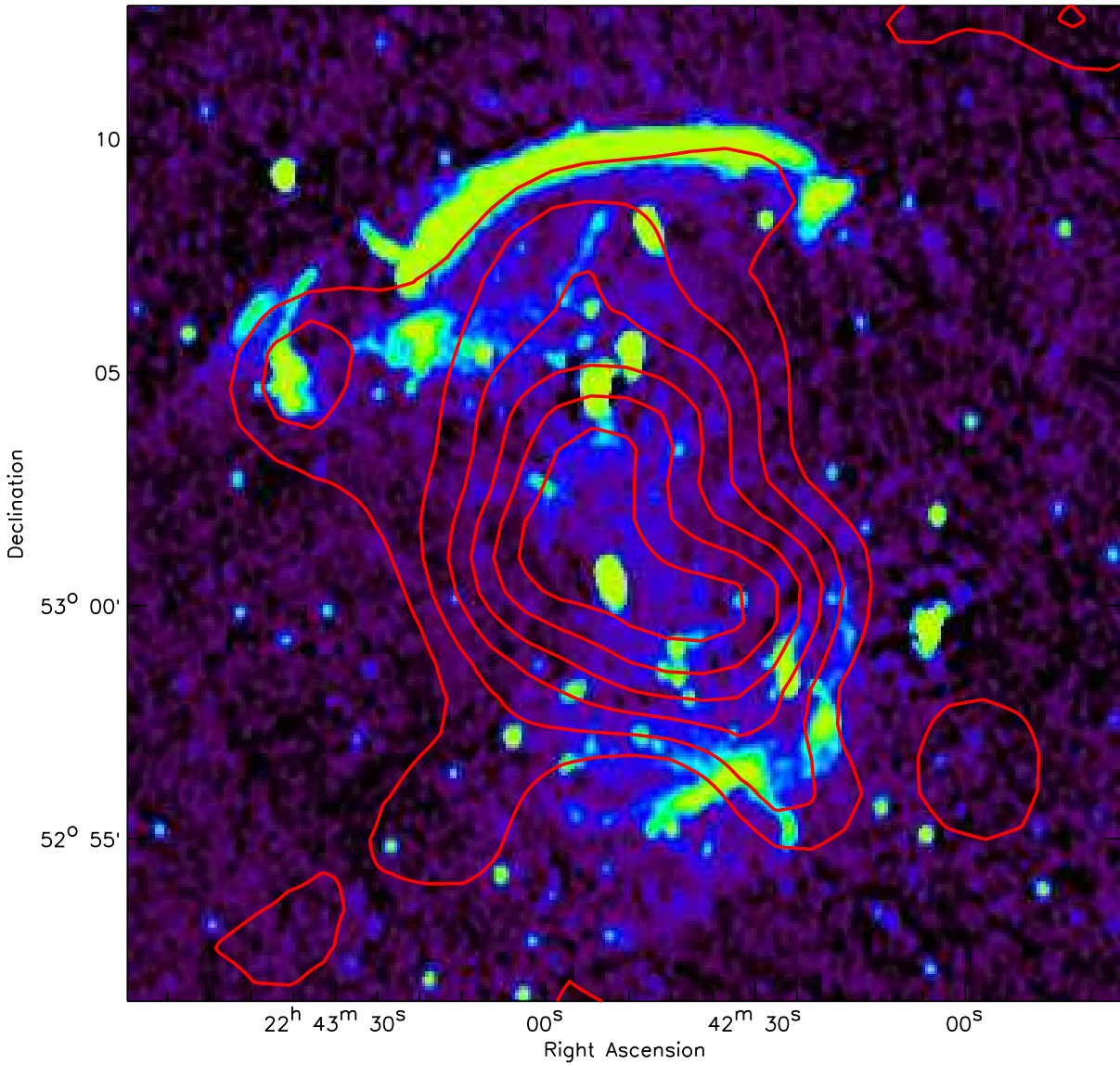


Figure 1: WSRT radio image at 1.4 GHz. The image has a resolution of $16.5 \text{ arcsec} \times 12.9 \text{ arcsec}$ and the rms noise is $19 \mu\text{Jy beam}^{-1}$. Red contours (linearly spaced) represent the X-ray emission from ROSAT showing the hot ICM.

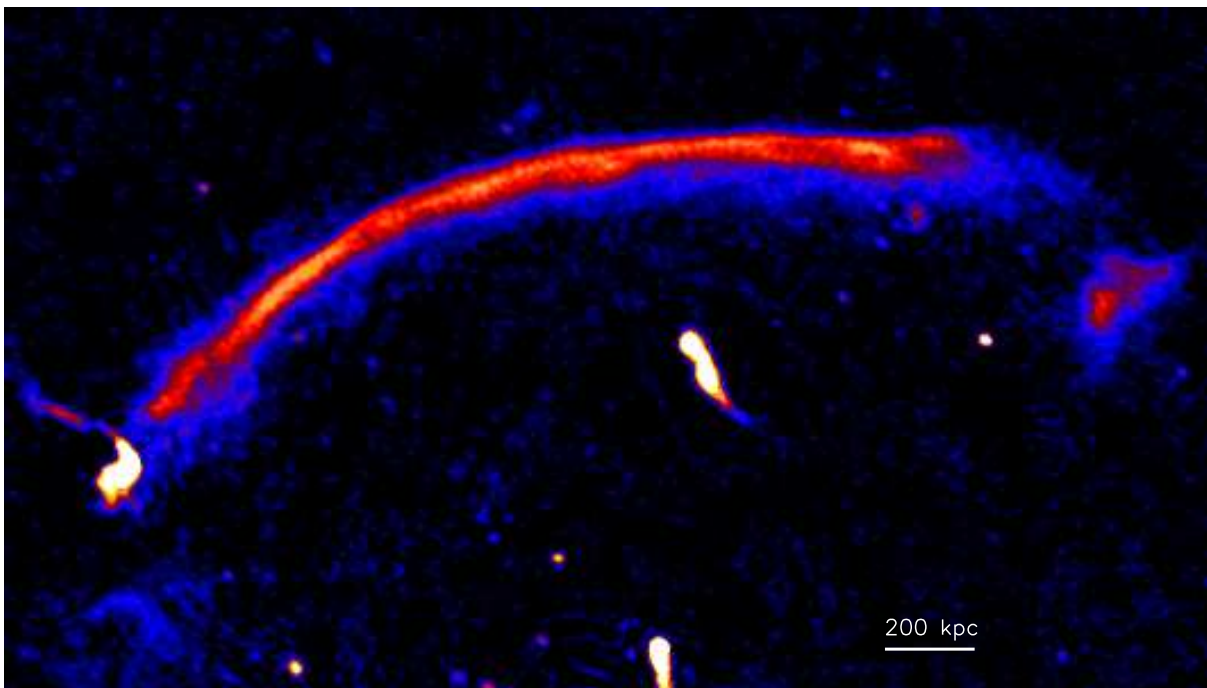


Figure 2: GMRT 610 MHz radio image. The image has a rms noise of $23 \mu\text{Jy beam}^{-1}$ and a resolution of $4.8 \text{ arcsec} \times 3.9 \text{ arcsec}$.

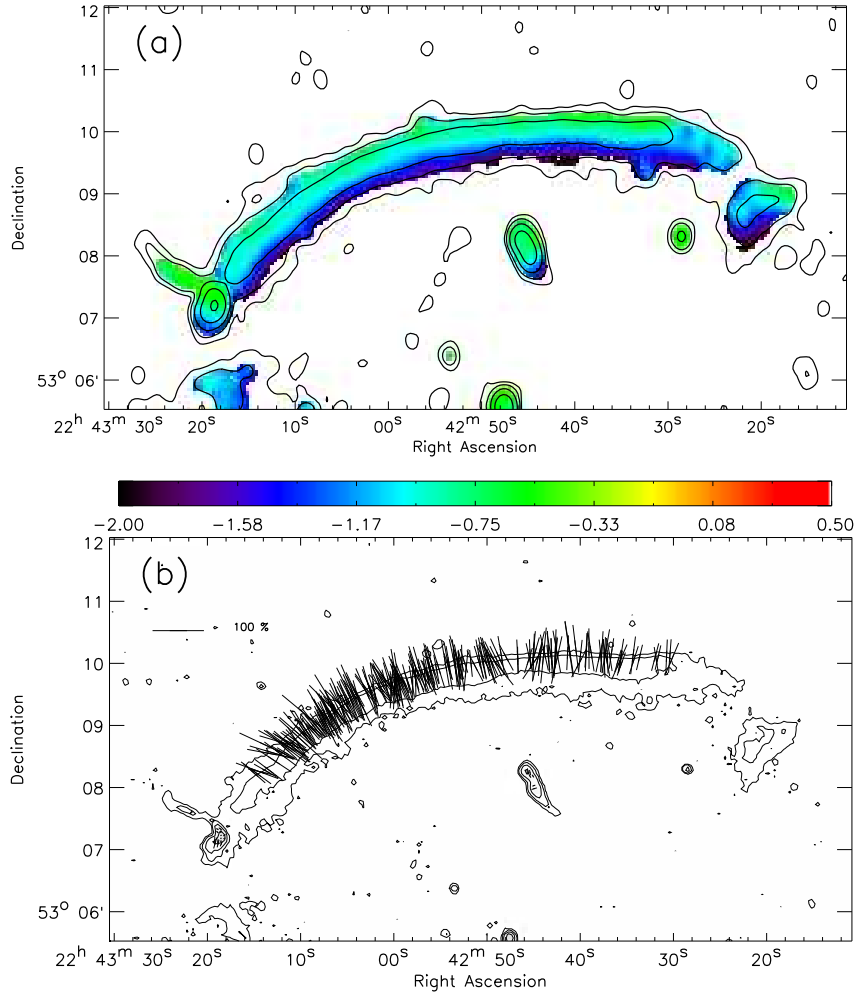


Figure 3: Radio spectral index and polarization maps. *a*: The spectral index was determined using matched observations at 2.3, 1.7, 1.4, 1.2, and 0.61 GHz, fitting a power-law radio spectrum to the flux density measurements. The map has a resolution of 16.7 arcsec \times 12.7 arcsec. Contours are from the WSRT 1.4 GHz image and are drawn at levels of $[1, 4, 16, \dots] \times 36 \mu\text{Jy beam}^{-1}$. *b*: The polarization electric field vector map was obtained with the VLA at a frequency of 4.9 GHz and has a resolution of 5.2 arcsec \times 5.1 arcsec. The contours are from Fig. 2 and are drawn at levels of $[1, 4, 16, \dots] \times 70 \mu\text{Jy beam}^{-1}$. The length of the vectors is proportional the polarization fraction, which is the ratio between the total intensity and total polarized intensity. A reference vector for 100% polarisation is drawn in the top left corner. The vectors were corrected for the effects of Faraday rotation using a Faraday depth of -140 rad m^{-2} determined from the WSRT 1.2 – 1.8 GHz observations.

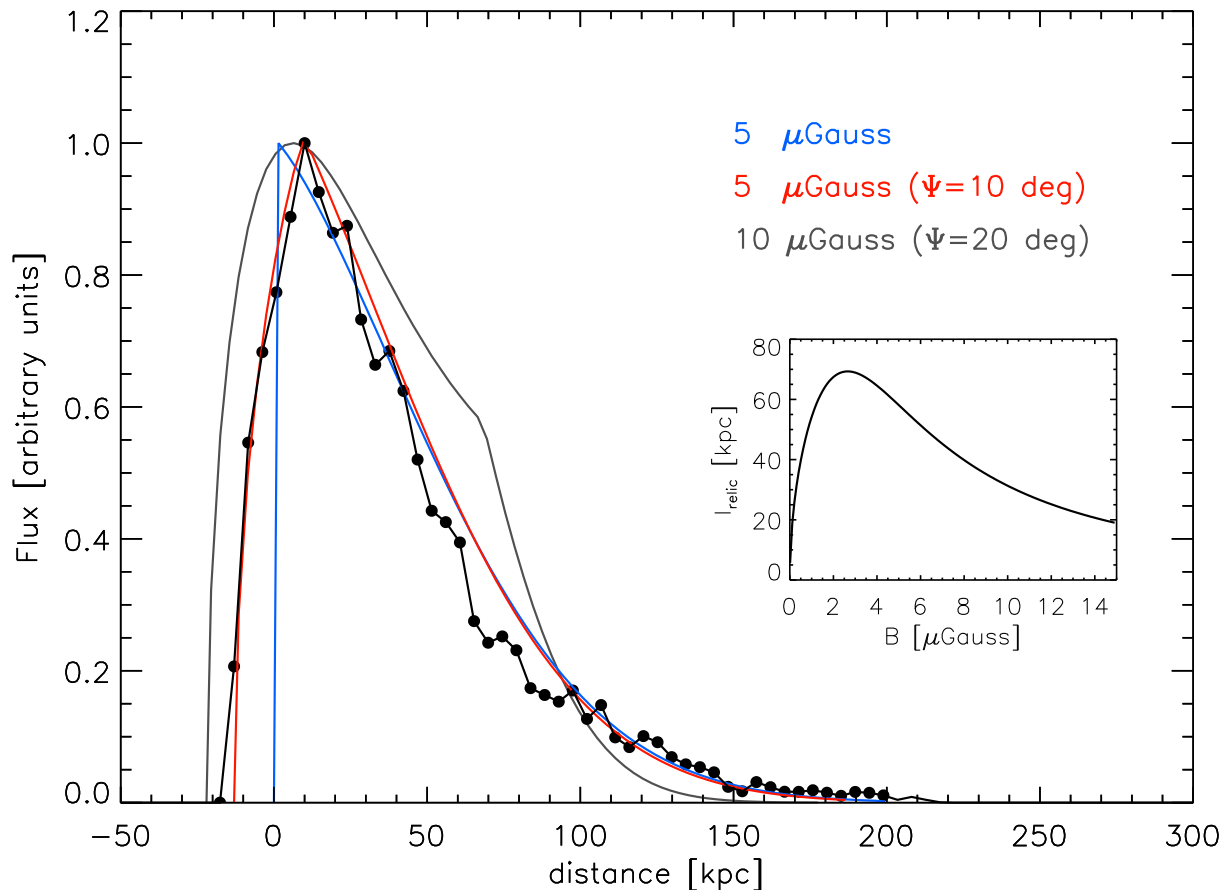


Figure 4: The deconvolved profile at 610 MHz, averaged over the full length of the relic, is shown by the solid black line and dots. Models for different magnetic field strengths and projection angles (Ψ ; i.e., the angle subtended by the relic into the plane of the sky) are overlaid. We used an equivalent magnetic field strength of the CMB at $z = 0.1921$ of $4.6 \mu\text{Gauss}$ and a downstream velocity of $1,000 \text{ km s}^{-1}$. The model (red) for $\Psi = 10 \text{ deg}$ and $B = 5 \mu\text{Gauss}$ provides the best fit. A model for $B = 5 \mu\text{Gauss}$ without any projection effects is overlaid in blue. For $\Psi > 15 \text{ deg}$ no good fit to the data could be obtained, as an example we have plotted the profile (grey) for $\Psi = 20 \text{ deg}$ and $B = 10 \mu\text{Gauss}$. (inset) The intrinsic width of the relic as function of magnetic field strength (Eq. 1), it shows that for a given width usually two solutions for the magnetic field strength can be obtained.

Supporting Online Material (SOM)

Materials and Methods

We carried out radio observations of CIZA J2242.8+5301 with the WSRT in the L-band (at 1.2, 1.4 and 1.7 GHz) and at 2.3 GHz recording full polarization products. The total integration time was 12 hr at 2.3, 1.2 and 1.7 GHz, and 30 hr at 1.4 GHz. The observations were spread out over various runs between March and November 2009. For each different frequency setup the total bandwidth was 160 MHz. The 160 MHz was further divided over 8 sub-bands (IFs) with 20 MHz bandwidth and 64 spectral channels. GMRT observations at 610 MHz were carried out with 32 MHz bandwidth in spectral line mode with 512 channels on November 19, 2009. The total integration time was 9 hr. Only RR and LL polarization, to create a total intensity image, were recorded. VLA C-array 4.9 GHz observations were taken on August 17, 2009 in single channel continuum mode recording all four polarization products. Total integration time was about 7.5 hr.

We reduced the data using AIPS¹ (Astronomical Image Processing System, NRAO) and CASA² (Common Astronomy Software Applications). After inspection for the presence of radio frequency interference and other problems, bad data was subsequently removed (i.e., “flagged”). Bandpass³ and gain calibration were carried out using several bright unresolved calibrator sources. The flux scale was set using standard primary calibrators (30, 31). For the WSRT observations the channel dependent polarization leakage terms were determined using a bright unpolarized calibrator source. The polarization angles were set using the polarized calibrators 3C138 and 3C286 for the WSRT and VLA observations. Subsequent rounds of self-calibration were carried out to improve the dynamic range of the images. Several bright nearby

¹<http://www.aips.nrao.edu/>

²<http://casa.nrao.edu/>

³only for the GMRT & WSRT observations

sources still limited the dynamic range in the 610 MHz GMRT image. These sources were subtracted from the data using the “peeling-method” (32, 33). The 610 MHz high-resolution image of the relic was made using robust weighting (34) set to -1.0 . A 610 MHz image of the cluster, with robust weighting set to 0.5, is shown in Fig. S5.

We made a radio spectral index map using images at 2.3, 1.7, 1.4, 1.2, and 0.61 GHz, fitting a power-law spectral index through the flux measurements. We limited the UV-ranges (to include only common UV-coverage) for the images that were used to compute the spectral index map. The spectral index map for the full cluster is shown in Fig. S6. Both the northern and southern relics show steepening of the spectral index towards the cluster center.

We used the technique of Rotation Measure Synthesis (35) to determine the Faraday depth of the northern relic. We found an average Faraday depth of about -140 rad m^{-2} and used that to correct for the effect of Faraday Rotation by de-rotating the electric/magnetic field vectors.

References and Notes

1. K. Roettiger, J. O. Burns, J. M. Stone, *Astrophys. J.* **518**, 603 (1999).
2. M. Hoeft, M. Brüggen, G. Yepes, S. Gottlöber, A. Schwobe, *Mon. Not. R. Astron. Soc.* **391**, 1511 (2008).
3. F. Miniati, T. W. Jones, H. Kang, D. Ryu, *Astrophys. J.* **562**, 233 (2001).
4. C. Pfrommer, T. A. Enßlin, V. Springel, *Mon. Not. R. Astron. Soc.* **385**, 1211 (2008).
5. L. O. Drury, *Reports on Progress in Physics* **46**, 973 (1983).
6. R. Blandford, D. Eichler, *Physics Reports* **154**, 1 (1987).
7. T. A. Ensslin, P. L. Biermann, U. Klein, S. Kohle, *Astron. Astrophys.* **332**, 395 (1998).

8. L. Feretti, *Advances in Space Research* **36**, 729 (2005).
9. J. Bagchi, F. Durret, G. B. L. Neto, S. Paul, *Science* **314**, 791 (2006).
10. T. E. Clarke, T. A. Ensslin, *Astron. J.* **131**, 2900 (2006).
11. A. Bonafede, *et al.*, *Astron. Astrophys.* **503**, 707 (2009).
12. A. Bonafede, G. Giovannini, L. Feretti, F. Govoni, M. Murgia, *Astron. Astrophys.* **494**, 429 (2009).
13. R. J. van Weeren, H. J. A. Röttgering, M. Brüggen, A. Cohen, *Astron. Astrophys.* **505**, 991 (2009).
14. R. J. van Weeren, *et al.*, *Astron. Astrophys.* **506**, 1083 (2009).
15. D. D. Kocevski, H. Ebeling, C. R. Mullis, R. B. Tully, *Astrophys. J.* **662**, 224 (2007).
16. W. Voges, *et al.*, *Astron. Astrophys.* **349**, 389 (1999).
17. G. K. Miley, *Astron. Astrophys.* **26**, 413 (1973).
18. D. Sijbring, A. G. de Bruyn, *Astron. Astrophys.* **331**, 901 (1998).
19. T. A. Enßlin, Gopal-Krishna, *Astron. Astrophys.* **366**, 26 (2001).
20. T. A. Enßlin, M. Brüggen, *Mon. Not. R. Astron. Soc.* **331**, 1011 (2002).
21. J. Vink, J. M. Laming, *Astrophys. J.* **584**, 758 (2003).
22. M. Markevitch, F. Govoni, G. Brunetti, D. Jerius, *Astrophys. J.* **627**, 733 (2005).
23. M. Markevitch, *Astrophys. J.* **504**, 27 (1998).
24. C. Ma, H. Ebeling, E. Barrett, *Astrophys. J. Lett.* **693**, L56 (2009).

25. M. Hoeft, M. Brüggen, *Mon. Not. R. Astron. Soc.* **375**, 77 (2007).
26. K. Nakazawa, *et al.*, *Publications of the Astronomical Society of Japan* **61**, 339 (2009).
27. A. Finoguenov, C. L. Sarazin, K. Nakazawa, D. R. Wik, T. E. Clarke, *Astrophys. J.* **715**, 1143 (2010).
28. T. E. Clarke, P. P. Kronberg, H. Böhringer, *Astrophys. J. Lett.* **547**, L111 (2001).
29. D. Ryu, H. Kang, E. Hallman, T. W. Jones, *Astrophys. J.* **593**, 599 (2003).
30. J. W. M. Baars, R. Genzel, I. I. K. Pauliny-Toth, A. Witzel, *Astron. Astrophys.* **61**, 99 (1977).
31. R. T. Perley, G. B. Taylor, VLA Calibrator Manual, *Tech. rep.*, NRAO (1999).
32. J. E. Noordam, *Society of Photo-Optical Instrumentation Engineers (SPIE) Conference Series*, J. M. Oschmann, Jr., ed. (2004), vol. 5489 of *Society of Photo-Optical Instrumentation Engineers (SPIE) Conference Series*, pp. 817–825.
33. H. T. Intema, *et al.*, *Astron. Astrophys.* **501**, 1185 (2009).
34. D. S. Briggs, , Ph.D. thesis, New Mexico Institute of Mining Technology, Socorro, New Mexico, USA (1995).
35. M. A. Brentjens, A. G. de Bruyn, *Astron. Astrophys.* **441**, 1217 (2005).
36. The WSRT is operated by ASTRON (Netherlands Institute for Radio Astronomy) with support from the Netherlands Foundation for Scientific Research (NWO). We thank the staff of the GMRT who have made these observations possible. The GMRT is run by the National Centre for Radio Astrophysics of the Tata Institute of Fundamental Research. The National

Radio Astronomy Observatory is a facility of the National Science Foundation operated under cooperative agreement by Associated Universities, Inc. R.J.v.W. acknowledges funding from the Royal Academy of Arts and Sciences (KNAW). The authors thank G. Brunetti for discussions.

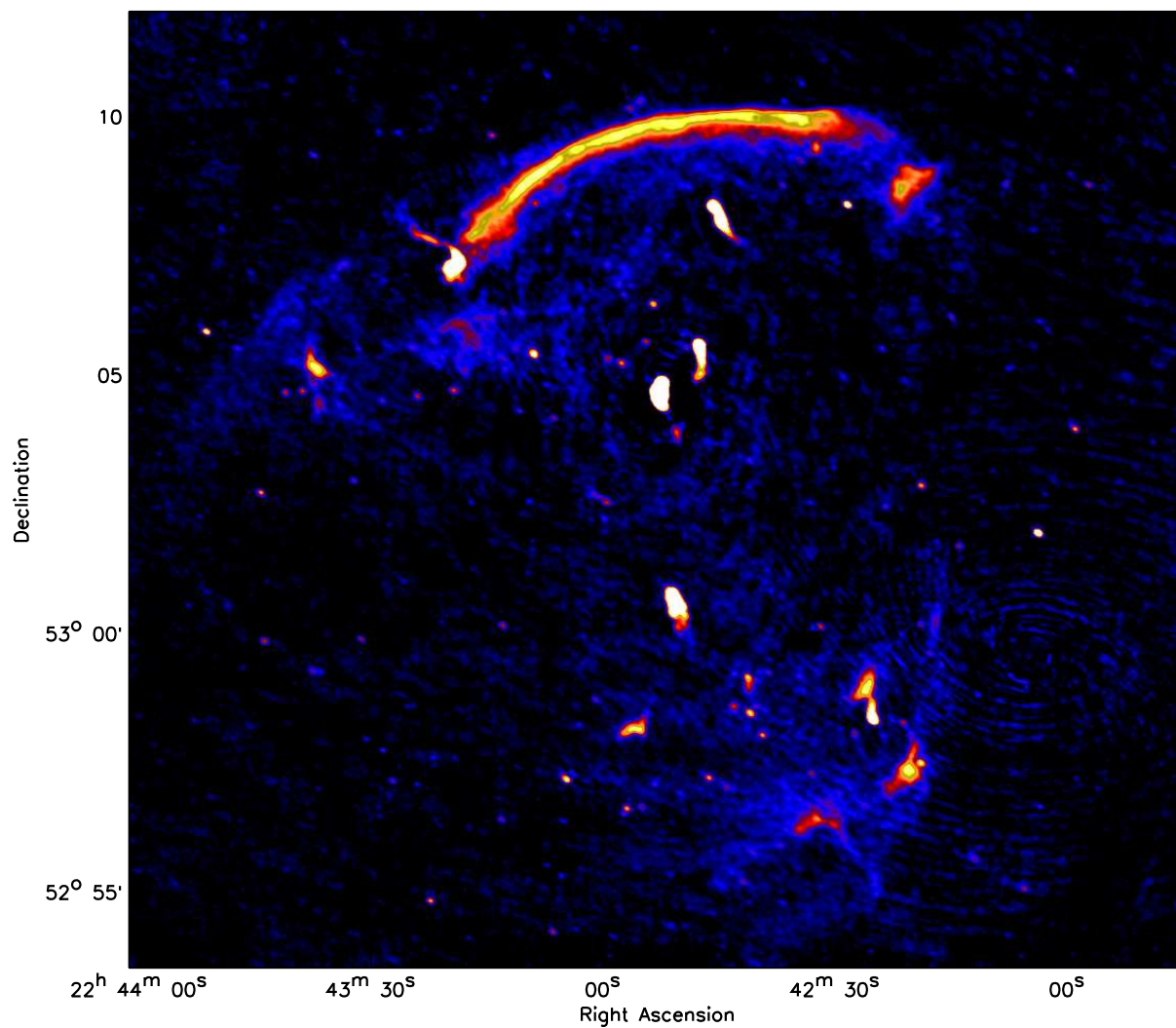


Figure S5: GMRT 610 MHz radio image with a resolution of $5.8 \text{ arcsec} \times 4.4 \text{ arcsec}$. The rms noise in the image is $24 \mu\text{Jy beam}^{-1}$.

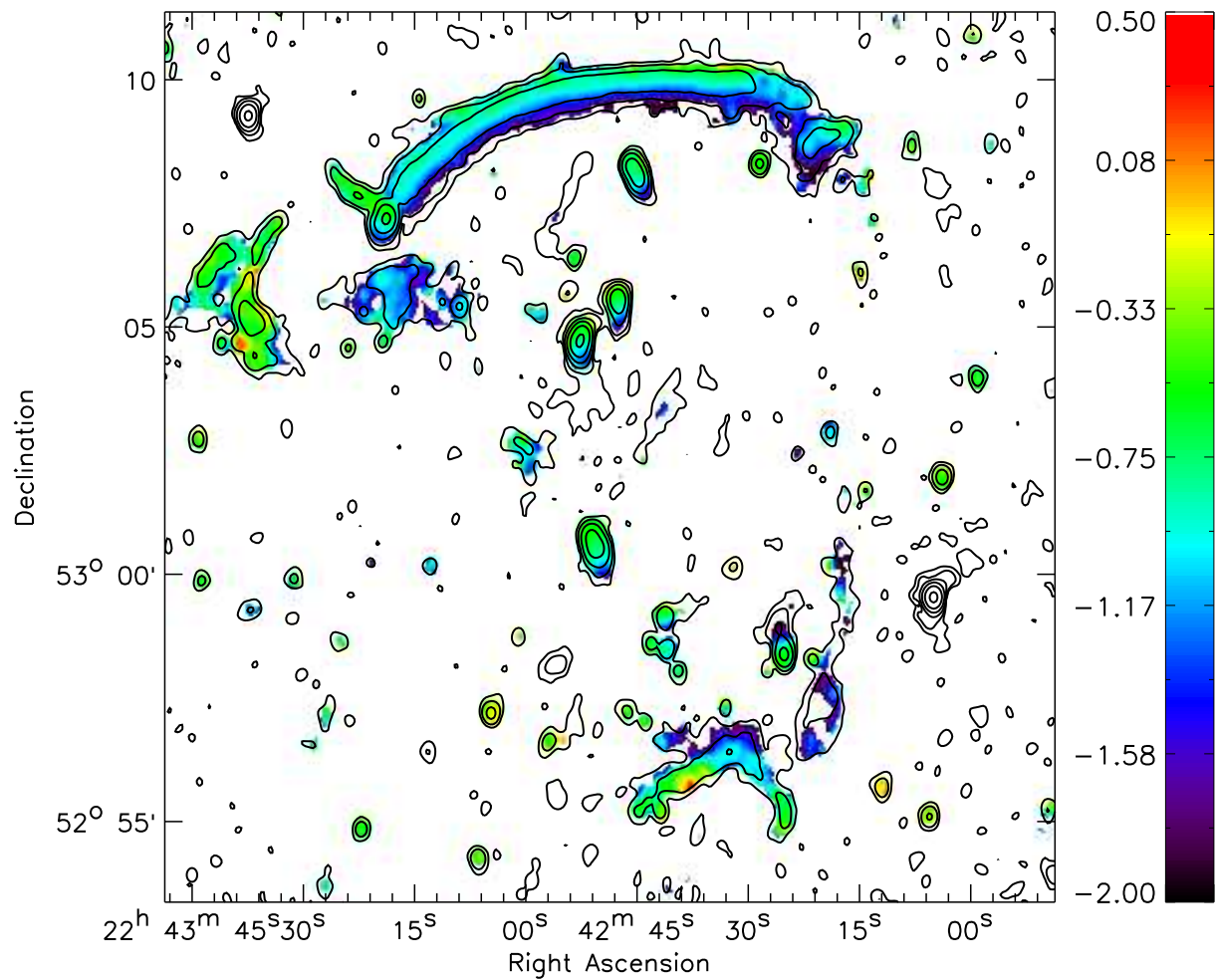


Figure S6: Radio spectral index map. The spectral index map has a resolution of 16.7 arcsec \times 12.7 arcsec. Contours are from the WSRT 1.4 GHz image and are drawn at levels of $[1, 4, 16, \dots] \times 57 \mu\text{Jy beam}^{-1}$.